



HAL
open science

Ash and gas discharge during open vent activity at El Reventador (Ecuador): explosion-style transitions driven by conduit capping

Freddy Vasconez Alban, Yves Moussallam, Philipson Bani, Jean Battaglia, Silvana Hidalgo, Mhammed Benbakkar, Andrew Harris, Diego Narvaez

► To cite this version:

Freddy Vasconez Alban, Yves Moussallam, Philipson Bani, Jean Battaglia, Silvana Hidalgo, et al.. Ash and gas discharge during open vent activity at El Reventador (Ecuador): explosion-style transitions driven by conduit capping. *Bulletin of Volcanology*, 2022, 84 (8), pp.77. 10.1007/s00445-022-01585-1 . hal-03874826

HAL Id: hal-03874826

<https://hal.science/hal-03874826v1>

Submitted on 28 Nov 2022

HAL is a multi-disciplinary open access archive for the deposit and dissemination of scientific research documents, whether they are published or not. The documents may come from teaching and research institutions in France or abroad, or from public or private research centers.

L'archive ouverte pluridisciplinaire **HAL**, est destinée au dépôt et à la diffusion de documents scientifiques de niveau recherche, publiés ou non, émanant des établissements d'enseignement et de recherche français ou étrangers, des laboratoires publics ou privés.



Distributed under a Creative Commons Attribution 4.0 International License

1 **Ash and gas discharge during open vent activity at El Reventador**
2 **(Ecuador): explosion-style transitions driven by conduit capping**

3 Vásconez, F.^{1,2}, Moussallam, Y.³, Bani, P¹., Battaglia, J.¹ Hidalgo, S.², Mhammed Benbakkar¹,
4 Harris, A.¹, Narváez, D.⁴

5
6 1- *Université Clermont Auvergne, CNRS, IRD, OPGC, Laboratoire Magmas et Volcans, F-63000 Clermont-Ferrand,*
7 *France*

8 2- *Instituto Geofísico, Escuela Politécnica Nacional, Ap. 17-01-2759, Quito, Ecuador*

9 3- *Lamont-Doherty Earth Observatory, Columbia University, New York, USA*

10 4- *Departamento de Geología, Escuela Politécnica Nacional, Ladrón de Guevara E11-253, Quito, Ecuador*

11

12 **Abstract**

13 Since the VEI 4 eruption of November 2002, El Reventador volcano (Ecuador) has been the
14 site of persistent open-vent activity characterized by frequent (hourly) Vulcanian –
15 Strombolian explosions and occasional (every few years) effusion of lava flows. The conduit
16 processes that sustain this continuous eruptive activity are still poorly understood. Here we
17 combine high temporal resolution thermal infrared imaging with seismic recordings and
18 DOAS-derived SO₂ fluxes focusing on a period of Vulcanian-style activity on 22-23 February
19 2017. Thermal imagery captured the emission and ascent dynamics of 26 plumes during the
20 observation period, including those fed by explosions and degassing episodes. While most
21 explosions have associated seismic signals, a few are marked by the absence of measurable
22 seismic activity. Degassing episodes also show very few associated seismic signals. Explosions
23 and degassing events seem to follow a sequence that can be explained by changes in the
24 conduit permeability associated with rapid (over time scales of minutes) rheological stiffening
25 of magma in the uppermost portion of the conduit to reduce degassing efficiency. Periods of
26 open-vent outgassing alternate with periods of conduit capping resulting in system
27 pressurization and leading to Vulcanian explosions that re-open the conduit allowing
28 outgassing to resume.

29

30 **Keywords:**

31 Vulcanian explosion, Strombolian explosion, Ash Venting, Open vent, Ecuador

32

33 **Resumen**

34 Desde la erupción VEI 4 de noviembre de 2002, el volcán El Reventador (Ecuador) ha sido
35 protagonista de una actividad persistente en sistema abierto (open-vent) caracterizada por
36 explosiones Vulcanianas — Estrombolianas frecuentes (en el orden de horas), y efusión de
37 flujos de lava y piroclásticos ocasionales (en el orden de meses a años). Los procesos en el
38 conducto que sustentan esta continua actividad eruptiva son aún poco conocidos. En este
39 trabajo combinamos el análisis de imagen térmica infrarroja en alta resolución temporal con
40 análisis de señales sísmicas y flujo de SO₂ obtenido mediante DOAS, enfocándonos en el
41 periodo de actividad tipo Vulcaniana ocurrida durante el 22 y 23 de febrero de 2017. Las
42 imágenes térmicas registraron la dinámica de emisión y ascenso de 26 plumas durante el
43 periodo de observación, incluyendo aquellas alimentadas por explosiones y episodios de
44 desgasificación. Aunque la mayoría de las explosiones tienen señales sísmicas asociadas, unas
45 pocas se caracterizan por la ausencia de actividad sísmica registrada en los sensores. Los
46 periodos de desgasificación también presentan señales sísmicas asociadas muy pequeñas. Las
47 explosiones y eventos de desgasificación parecen seguir una secuencia o ciclo que puede ser
48 explicado por cambios en la permeabilidad del conducto asociados a una variación rápida (en
49 la escala de minutos) de la rigidez del magma en la parte más somera del conducto, con lo que
50 se limitaría la eficiencia de la desgasificación. La alternancia de periodos de desgasificación en
51 conducto abierto con periodos de taponamiento del conducto da lugar a una presurización
52 del sistema derivando en explosiones Vulcanianas que vuelven a abrir el conducto, lo que
53 reanuda la secuencia con un nuevo proceso de desgasificación.

54

55

56 **Introduction**

57 Vulcanian eruptions involve short-lived intermittent explosive events that can continue for
58 periods of years (Mercalli 1907). They are small to moderate in size, feeding eruptive columns
59 typically reaching less than 10 km height, but which can collapse to generate pyroclastic flows
60 (e.g., Marchetti et al. 2009; Yokoo 2009; Hall et al. 2015). Numerous recent volcanic eruptions
61 have been catalogued as Vulcanian including at Sakurajima volcano in Japan since 1955 (Miwa
62 and Toramaru 2013); Fuego volcano in Guatemala in 1978 (Wilson and Self 1980); Soufrière
63 Hills volcano in Montserrat in 1997 (Formenti et al. 2003); Tungurahua volcano in Ecuador in
64 2013-2014 (Hidalgo et al. 2015; Hall et al. 2015; Battaglia et al. 2019; Gaunt et al. 2020); and
65 El Reventador volcano in Ecuador since 2002 (Lees et al. 2008). Such Vulcanian eruptions can
66 either be caused by phreatomagmatic or purely magmatic processes (cf. Clarke et al. 2015),
67 but the classic model for magmatic Vulcanian eruptions is that they originate from the rupture
68 of a gas-impermeable plug formed in the upper part of a magma-filled conduit (e.g., Fagents
69 and Wilson 1993; Self et al. 1979; Sparks 1997; Woods 1995). Vulcanian eruptions are most
70 commonly found at volcanoes erupting magmas of basaltic andesite to dacitic composition
71 and usually emit only small amounts of ejecta ($<1 \text{ km}^3$; Morrissey and Masting 1999). The
72 velocity at which the material is expelled from the vent during Vulcanian explosions has been
73 linked to the amount of gas involved in the event (Self et al. 1979; Wilson and Self 1980;
74 Formenti et al. 2003; Clarke et al. 2015).

75

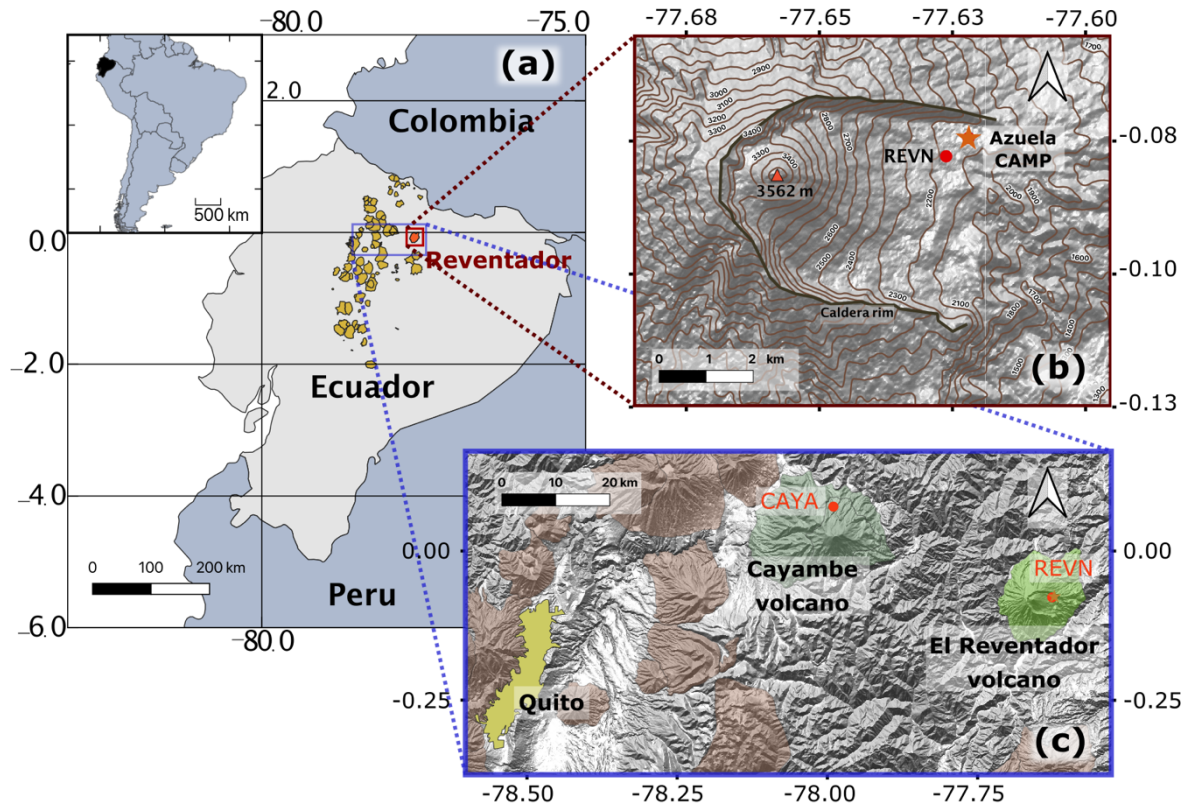
76 El Reventador volcano is a stratovolcano located on the rear-arc zone at the boundary of the
77 Eastern cordillera and Amazon basin in Ecuador (Fig. 1a). Its currently active cone is located
78 inside a horseshoe-shaped amphitheater that is 4 km wide (north-south) and 6 km long
79 (northwest – southeast) and open to the southeast (Fig. 1b). Since 1541, this volcano has
80 experienced more than 20 eruptive episodes (Siebert et al. 2011; Naranjo et al. 2016) of which
81 seven occurred in the twentieth century (Hall et al. 2004). The first and the longest episode of
82 the twentieth century took place from 1898 to 1912, and subsequent eruptive episodes had
83 variable durations of up to 3 years, each separated by periods of around 12 years of
84 quiescence. The last eruptive episode of the twentieth century ended in 1976. All of these
85 eruptive episodes were “moderate” to “moderate-large” in scale (i.e., VEI 2-3), with
86 Strombolian to Vulcanian eruptive styles (cf. Newhall and Self 1982), and produced blocky lava
87 flows, small-volume pyroclastic and debris flows, and ash fallout (Hall et al. 2004; Samaniego

88 et al. 2008). El Reventador's most recent and still ongoing (at the time of writing) eruptive
89 episode began in November 2002 with a VEI 4 explosion that destroyed the summit and crater
90 of the cone, leaving deep notches on the northern and southern margins of the summit, and
91 produced an eruptive column that rose up to 16-17 km above the crater (Hall et al. 2004).
92 Pyroclastic flows were produced and reached the Coca river, ~9 km to the east of the active
93 vent, destroying the main oil pipelines and the road leading to the oilfields of Ecuador.
94 Ecuador's capital city, Quito, located ~100 km to the west (Fig. 1c), had to close down its
95 international airport for eight days to allow ash clean-up operations that required removal of
96 1-2 mm ash produced by the intense ash fall of November 3 (Hall et al. 2004). During the first
97 year after the paroxysmal event, two lava flows were emplaced from the summit and from a
98 lateral vent in the southeastern cone flank (Samaniego et al. 2008; Naranjo et al. 2016). After
99 around 1 year of quiescence, in 2004, new lava flows formed, followed by the alternation of
100 effusive and mildly explosive periods (Lees et al. 2008; Ortiz et al. 2020). By 2015, the volcanic
101 cone had a similar shape to that which existed before 2002 (Ortiz et al. 2020). Between 2016
102 and 2018, Almeida et al. (2019) documented a series of morphologic changes in the upper
103 edifice, including the existence of two active vents in January 2016, a lateral eruption in June
104 2017, and a partial summit collapse in April 2018. By the time of our observations in February
105 2017, five effusive episodes had been identified by Naranjo et al. (2016) and Arnold et al.
106 (2017). The discharge rate within each of the effusive periods was variable, with a general
107 decreasing trend from one period to the next (Lees et al. 2008; Naranjo et al. 2016; Arnold et
108 al. 2017). From 2012 through 2020, and continuing during effusive episodes, a variable
109 number of explosions (up to 50 per day) were recorded by the local monitoring network
110 operated by the Instituto Geofísico of Escuela Politécnica Nacional (IGEPN) (cf. Ramon et al.
111 2021). These transient explosions typically produced ash columns of variable ash content and
112 height, ascending up to 2 km above the summit crater (e.g., Instituto Geofísico 2010, 2018,
113 2019). Similar activity has been observed at other open-vent andesitic through dacitic systems
114 as, for example Sangay in Ecuador (Johnson and Lees 2000), Karymsky in Kamchatka (Johnson
115 and Lees 2000) and Santiaguito in Guatemala (Johnson et al. 2008; Sahetapy-Engel et al. 2008;
116 Sahetapy-Engel and Harris 2009). Models proposed to explain the generation of such
117 explosions include accumulation of gas under a near-surface structure, i.e., a plug or a
118 viscoelastic lava dome acting as pressure valve, that is released by the mechanical failure of
119 the blocking structure (Johnson and Lees 2000; Johnson et al. 2008). A second model explains

120 ash eruptions at such open-vent system as being generated by slip events to cause shear-
121 induced magma fragmentation at the conduit boundaries around the ascending dacite plug
122 (Gonnermann and Manga 2003; Bluth and Rose 2004; Sahetapy-Engel et al. 2008).

123

124 Here, our aim is to analyze the ongoing volcanic activity at El Reventador to propose an
125 explanation for the generation of the Vulcanian explosions and the associated plume
126 dynamics. We present two-hours of quasi-continuous thermal video to describe the evolution
127 of the activity, the duration of each explosion and propose a classification based on explosion
128 characteristics. The flux of SO₂ emitted during the same period was measured by scanning
129 DOAS (Differential Optical Absorption Spectroscopy; Platt and Stutz 2008) while the seismic
130 activity was recorded by broadband seismometers at both proximal (~4 km) and distal (~45
131 km) locations (REVN and CAYA, Fig. 1c). Together, these observations suggest a sequence of
132 four phases of activity reflecting evolving conditions in the shallow conduit. The sequence
133 starts with no degassing and pressure build-up and is followed by destruction of a cap during
134 a Vulcanian explosion. Thereafter, there is a phase of open-vent degassing punctuated by
135 small Strombolian explosions as gas slugs episodically reach the surface. Afterwards, a new
136 plug develops by cooling of the uppermost magma in the conduit, causing gas emissions to
137 decrease until the system becomes fully plugged again; thereafter the cycle recommences.



138

139 **Fig. 1** (a) Location of El Reventador in Ecuador where yellow symbols are volcanoes active during the
 140 Holocene. Note that El Reventador is located to the east of the eastern side of the cordillera in Ecuador.

141 (b) Enlargement on the current active cone at El Reventador, where “Azuela CAMP” is the site from
 142 which measurements were made and “REVN” is the proximal seismic station.

143 (c) Map of the region to the West of El Reventador showing the location of the distal seismic station (“CAYA”), located in the
 144 northern flank of Cayambe volcano, and the city of Quito.

145

146

147 **Methodology**

148 The dataset analyzed here was acquired during a field campaign in February 2017 and consists
149 of three types of recordings: (1) Thermal infrared video, (2) Scanning DOAS for SO₂ flux, and
150 (3) Seismic. These we used together with visual observations and major element composition
151 analysis of the emitted ash, which was simultaneously collected with the geophysical data sets
152 (cf. Thivet et al. 2021).

153

154 **Thermal analysis**

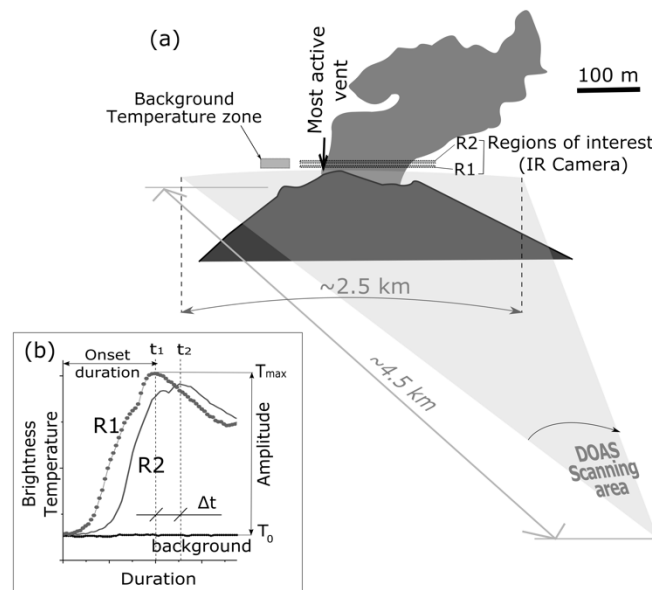
155 Thermal videos were recorded from the Azuela CAMP site, located 4.5 km to the ENE of the
156 active crater (latitude 0.07577S, longitude 77.62473W, altitude 2160 m a.s.l., Fig. 1b). We used
157 an Optris PI 640 thermal infrared (8 – 14 μm) camera with a lens that produces a field of view
158 of 15° × 11° and a 640 × 480 pixel image. The pixel size corresponding to a 4.5 km distance to
159 the summit is 1.85 m. Videos of explosive events were captured at a rate of 32 frames per
160 second (fps), with the thermal recording covering a quasi-continuous period of 2 hours, from
161 23h14 UTC on February 22 to 01h33 UTC on February 23.

162

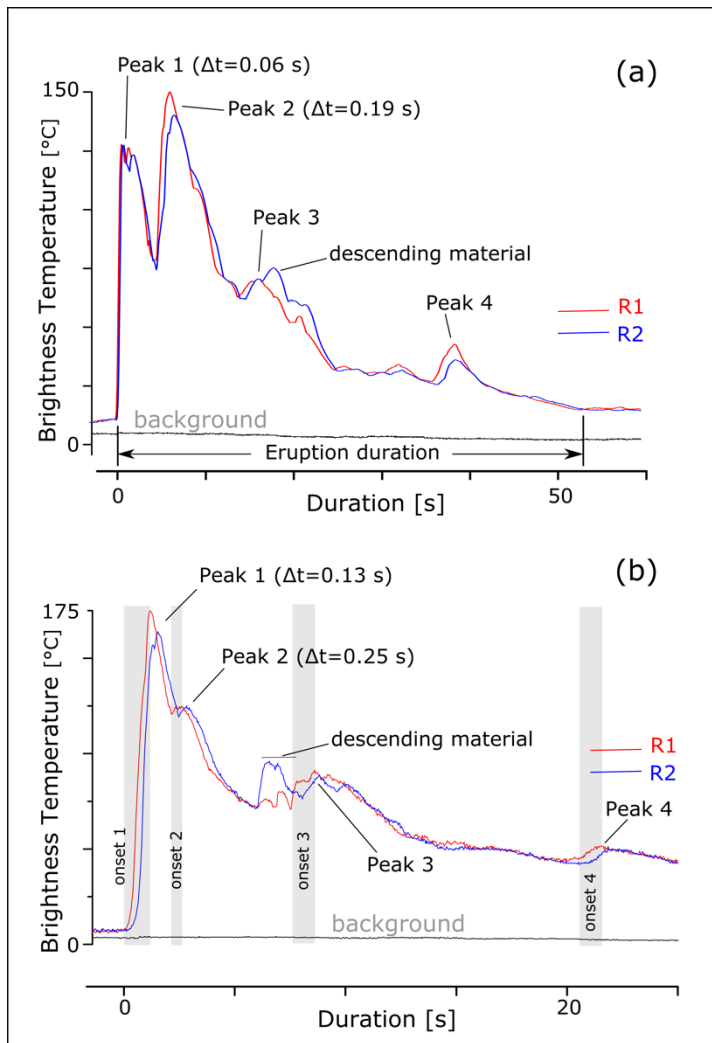
163 To track and define thermal waveforms associated with the explosive events, a region of
164 interest was defined directly above the crater rim (R1, Fig. 2) to capture any emission of hot
165 fragments, ash and/or hot gases (Harris and Ripepe 2007a). A second region of interest (R2)
166 was placed 1.85 or 3.7 m vertically above R1 (Fig. 2) to determine the ascent velocity from the
167 delay in waveform onset between R1 and R2 (Sahetapy-Engel et al. 2008). Retrieving the
168 kinetic temperature of fragments and hot gasses requires a correction for atmospheric
169 absorption and emission, as well as emissivity effects (Harris 2013). Here, since we are
170 interested in the relative changes of thermal signal instead of the absolute kinetic
171 temperatures, and given minimal atmospheric effects at these altitudes (cf. Harris 2013), we
172 present our data in terms of uncorrected brightness temperatures (cf. Matsushima 2005; Bani
173 et al. 2013). The thermal amplitude is defined as the difference between the peak
174 temperature and background temperature in any waveform (Harris and Thornber 1999;
175 Ripepe et al. 2005). The timestamps for the time series were recorded using the operating
176 computer, cross calibrated to GPS time.

177

178 Durations of ash and/or gas venting were also obtained from these thermal time series. In
 179 most cases, the starting and ending points of an explosion are clearly defined (Fig. 3). In some
 180 cases, however, when there is a phase of slow ash dispersal at the end of the event, the
 181 definition of the end of the explosion becomes ambiguous. In such a situation, we define the
 182 end of the event as the instant when the temperature inside the region R1 drops below the
 183 limit set as twice the background temperature (Fig. 3).



184
 185 **Fig. 2** (a) Layout of the measurement setup. The thermal camera and the DOAS were located 4.5 km
 186 to the east of the active cone. Two regions of interest (R1 and R2) are placed directly above the crater
 187 to track any fluctuation in the temperature due to hot material exiting the vent. The temperature of
 188 the background was also measured in the clear sky region as indicated. Also marked is the horizontal
 189 scanning plane covered by the DOAS. (b) Timeseries obtained from R1 and R2. Definition of the time
 190 delay between the peak temperature recorded at R1 (t_1) and R2 (t_2) as used to calculate ascent speed,
 191 onset time (the time to move from background temperature, T_0 , to peak temperature, T_{max}), and
 192 thermal amplitude ($T_{max}-T_0$) (after Harris and Ripepe, 2007). Example is from the onset of explosion 4.



193
 194 **Fig. 3** Time series from regions of interest R1 (red line) and R2 (blue line) for explosions (a) 11 and (b)
 195 13. When hot pulses of ash and/or gas transit through R1 and R2, they trigger an impulsive increase in
 196 temperature, followed by a slower decrease. Objects first cross R1 and then R2, causing a delay
 197 between the two waveforms. Peaks that appear first in R2 before R1 correspond to hot bombs and
 198 blocks falling back to the ground. The time delay between a peak at R1 and its corresponding pike in
 199 R2 is signaled as Δt (Fig.2).

200

201 **SO₂ flux**

202 To estimate SO₂ flux we used a scanning DOAS from a fixed position at the Azuela CAMP site
 203 (Fig. 2). During measurements, the plume rose several hundred meters vertically above the
 204 summit before drifting to the east, enabling both horizontal and vertical scanning of the
 205 plume. Thirty-three spectra per scan were collected with a step angle of 0.9°, covering a
 206 horizontal scanned length of ~2.5 km in the horizontal configuration (Fig. 2a). The angular
 207 resolution was maintained when switching to the vertical configuration. The spectrometer

208 used was an Ocean Optics USB2000+ with a spectral range of 290-440 nm and a spectral
209 resolution of 0.5 nm FWHM. The SO₂ column amounts (ppm.m) were retrieved using standard
210 DOAS calibration and analysis procedures (Platt and Stutz 2008). Reference spectra included
211 in the non-linear fit were obtained by convolving high resolution SO₂ (Bogumil et al. 2003) and
212 O₃ (Voigt et al. 2001) cross sections with the instrument line shape. A Fraunhofer reference
213 spectrum and Ring spectrum, calculated in DOASIS (DOAS Intelligent System; Kraus 2006),
214 were also included in the fit. Measurements were made between 13h21 and 14h15, UTC, on
215 February 23, 2017. The plume speed was calculated following the method described above in
216 the paragraph of thermal analysis but also applied to periods of passive degassing. The plume
217 transport speed relative error is conservatively assumed to be around 30–35%, which is
218 towards the higher end of the range of past estimates (e.g., Arellano et al. 2008; Bani 2012;
219 Bani et al. 2013b).

220

221 **Seismicity**

222 We used two broadband seismic stations from the permanent monitoring network of the
223 IGEPN: REVN located 4 km from the summit of El Reventador and CAYA located 45 km to the
224 west on the northern flank of Cayambe volcano (Fig. 1). Both stations are equipped with
225 Trillium Compact 120s sensors with Q330 Kinometrics digitizers. Data are recorded with a 100
226 Hz sampling frequency. Station REVN records both explosion quakes and tremors from El
227 Reventador. Instead station CAYA, while normally used to monitor the activity at Cayambe
228 volcano, also records the most energetic explosion-quakes from El Reventador.

229

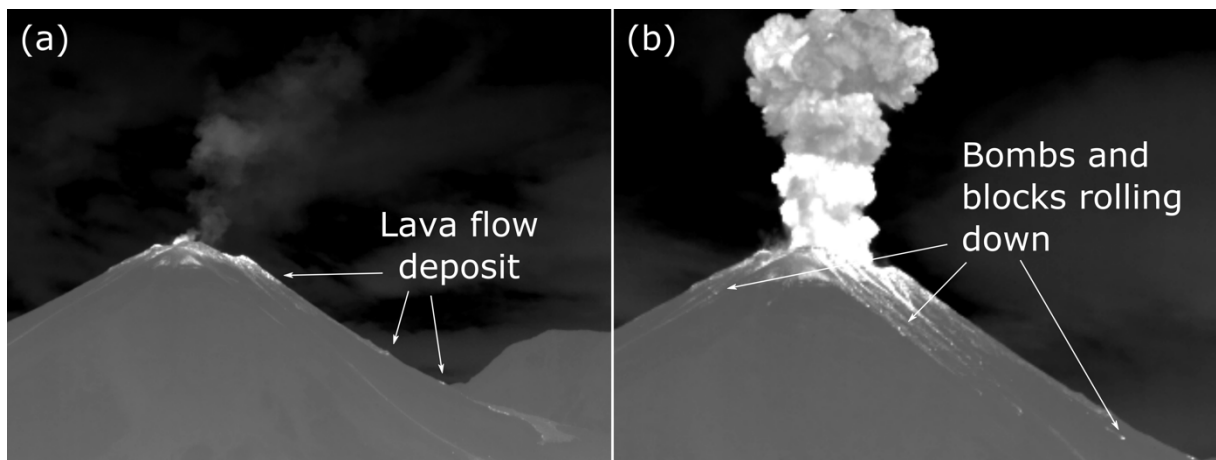
230 **Ash composition**

231 Ash fall deposited during the observation period was collected and analyzed for major
232 element bulk composition. To do this, 100 mg of sample was mixed with 300 mg of LiBO₂,
233 melted in an induction oven at 1050 °C for 4.5 min using graphite crucibles. The resulting glass
234 beads were then dissolved in a solution of deionized water and nitric acid (200 ml) and finally
235 diluted by a factor of 2000. The solutions were analyzed by ICP-AES (An ULTIMA-C Horiba
236 scientific, Jobin-Yvon spectrometer was used) at the Laboratoire Magmas et Volcans in
237 Clermont-Ferrand (France).

238

239 **Results**

240 The activity we observed at El Reventador on 22 and 23 February 2017 was dominated by
241 intermittent explosions that fed ash plumes up to about one kilometer above the summit,
242 before detaching and being pushed to the east by the prevailing wind. The activity reports of
243 IGEPN show a mean of 40 explosions per day and a similar number of long-period (LP) seismic
244 events were recorded by station REVN. A small area of incandescent lava could be seen on the
245 upper part of the northern flank of the cone. Most of the ejected blocks and bombs remained
246 within the summit crater; although, during larger explosions, incandescent blocks were seen
247 rolling down the flanks of the cone (Fig. 4).



248
249 **Fig. 4** Thermal infrared images of the summit area. (a) A small area of the deposit of a recent lava flow
250 was recognizable on the northern flank. (b) During energetic explosions, most of the ejected blocks
251 and bombs rolled down the flanks of the cone.

252 **Thermal data**

253 Thirteen explosions of variable thermal amplitude were recorded over the 2-hour
254 measurement period. Another 13 less energetic degassing events were also recorded during
255 this observation period. All thermal infrared videos are available in the Electronic
256 Supplementary Material (ESM Video 01-Video 19).

257
258 Thermal amplitudes of the explosions varied between 40°C for the less energetic (minor)
259 events (explosion 7) and up to 263 °C for the most energetic (major) events (explosion 3).
260 Minor explosions only lasted for around 10 s, while major explosions persisted for up to 140
261 s. The 32 Hz acquisition rate of the thermal recording allowed a detailed thermal waveform to
262 be generated for each event, highlighting successive thermal peaks within each explosive

263 discharge. Figure 5 shows an example of a sequence of thermal images acquired during an
264 explosion with the corresponding thermal waveform. In this example, at least 11 thermal
265 peaks are recorded over the 30 s of duration of the event highlighting a series of explosive
266 pulses (cf. Harris et al. 2008). Generally, as in the Figure 5 waveform, the highest thermal
267 amplitude recorded during any single explosion corresponded to the first or second peak, and
268 amplitudes thereafter declined (cf. Fig. 3), consistent with a waning emission.

269

270 The time delay between consecutive peaks varies from 0.03 to up to 0.6 s, implying a decrease
271 in velocity with increased delay (Fig. 2b). For our travel distance between R1 and R2 of 3.7 m,
272 this gives velocity end members of 3 to 120 m s⁻¹, with an average of 27 m s⁻¹. We see from
273 Figure 3 that the delay between any two peaks increases with time during any individual
274 event, increasing from 0.06 to 0.19 s in Figure 3a and from 0.13 to 0.25 s in Figure 3b. This is
275 consistent with a decrease in emission velocity with time, from 30 to 10 and 20 to 7 m s⁻¹ in
276 the two cases, respectively. The decay in thermal amplitude is also consistent with an event
277 that decays in energy with time.

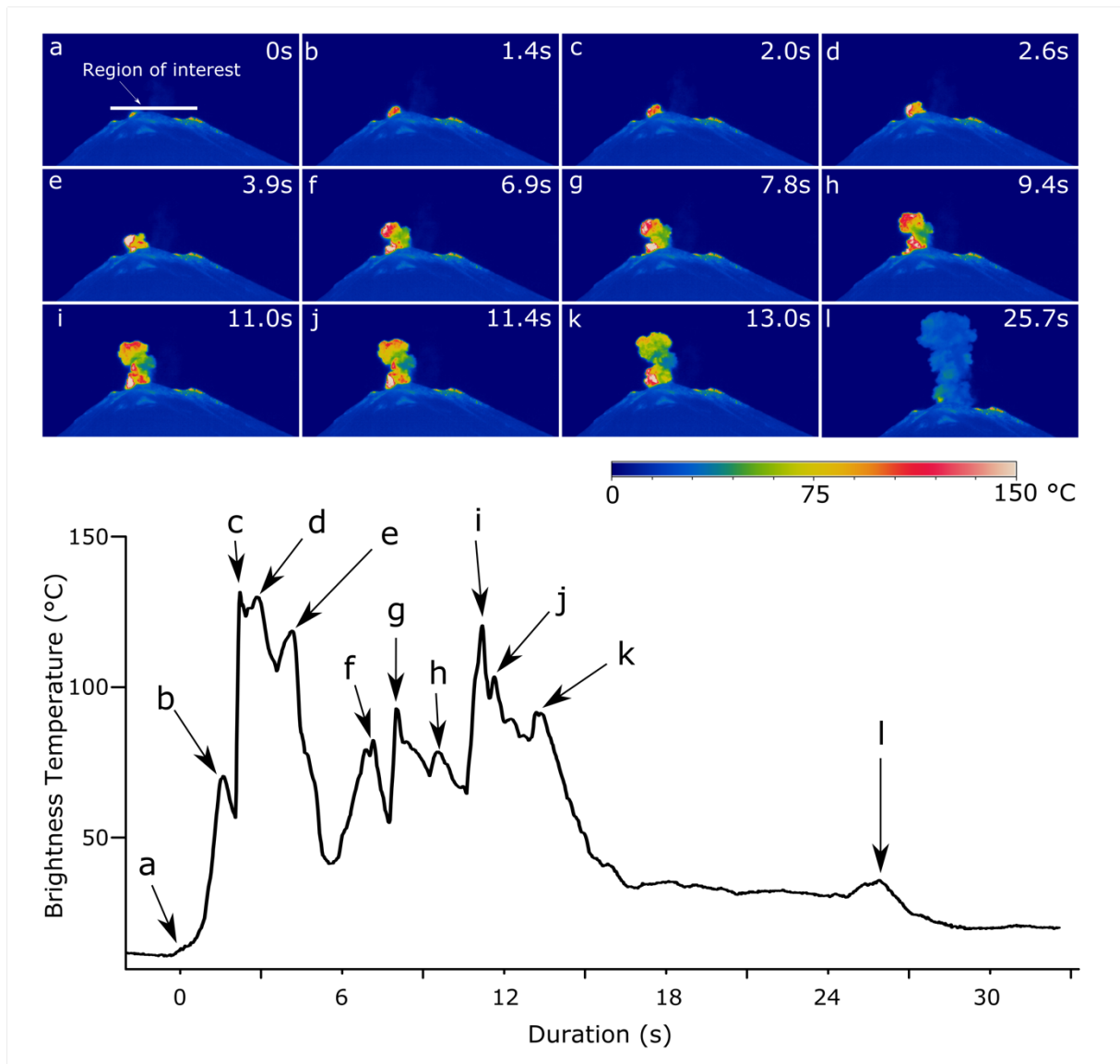
278

279 On the basis of thermal waveform (i.e., their thermal amplitude and duration), we classified
280 the recorded emissions into three types (Fig. 6).

- 281 • Type A (Fig. 6a), is characterized by the highest thermal amplitudes (263 °C), longest
282 durations (140 s) and highest plumes (> 800 m).
- 283 • Type B (Fig. 6b), is characterized by moderate thermal amplitudes (175 °C), durations
284 of around 25 s and plume heights reaching up to 400 m.
- 285 • Type C (Fig. 6c) is characterized by the lowest thermal amplitudes (100 °C), durations
286 of about 15 s and plume heights of up to 300 m.

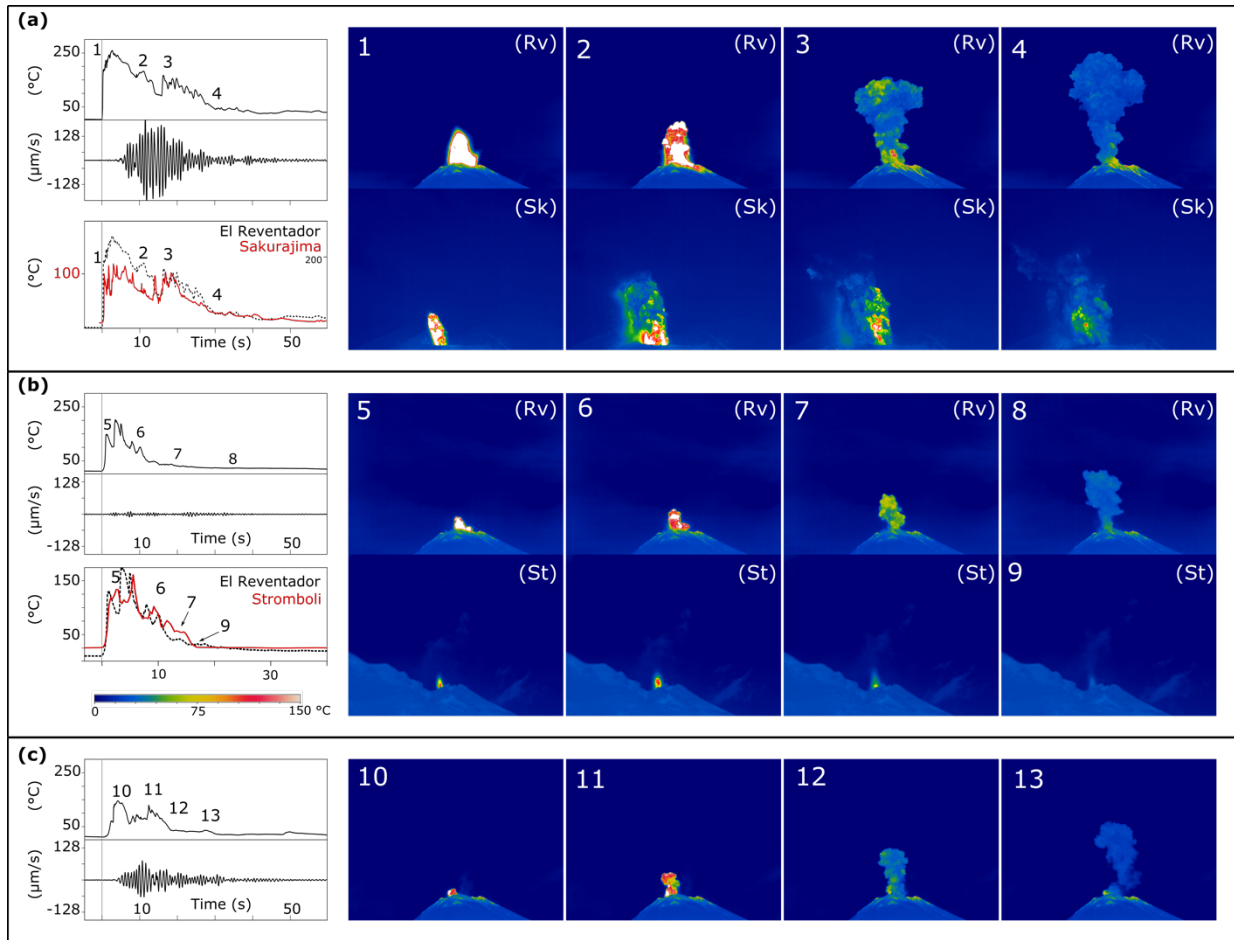
287 This all implies a decrease in energy between each event type. We find that each event type
288 tends to occur in a specific sequence (Fig. 7a). Type B and C events tend to occur together,
289 with Type B punctuating clusters of repeated, at the rate of 0.2-0.7 Hz, Type C events (Fig. 7b)
290 Such sequences are typically followed by explosion free periods (Fig. 7c), which are terminated
291 by single, discrete Type A events (Fig. 7d). Explosion free periods show the existence of very
292 low amplitude (10 °C) single peaked waveforms of 12 – 20 s in duration and which are
293 associated with exhalations of gas (Fig. 7c). Within the sequence of Figure 7e, three individual

294 events of around 30 s in duration occurred with one minute delays, with decreasing thermal
295 amplitudes.



296
297 **Fig. 5** Sequence of thermal images acquired during explosion 2 and the corresponding thermal
298 waveform for the Region of Interest labelled in (a). Labelled letters on the waveform related to the
299 location of thermal video frames (a) through (l). The eruption lasted 30s with 11 peaks each associated
300 with a burst of material passing through the ROI (cf. Harris et al. 2008).

301



302

303

304

305

306

307

308

309

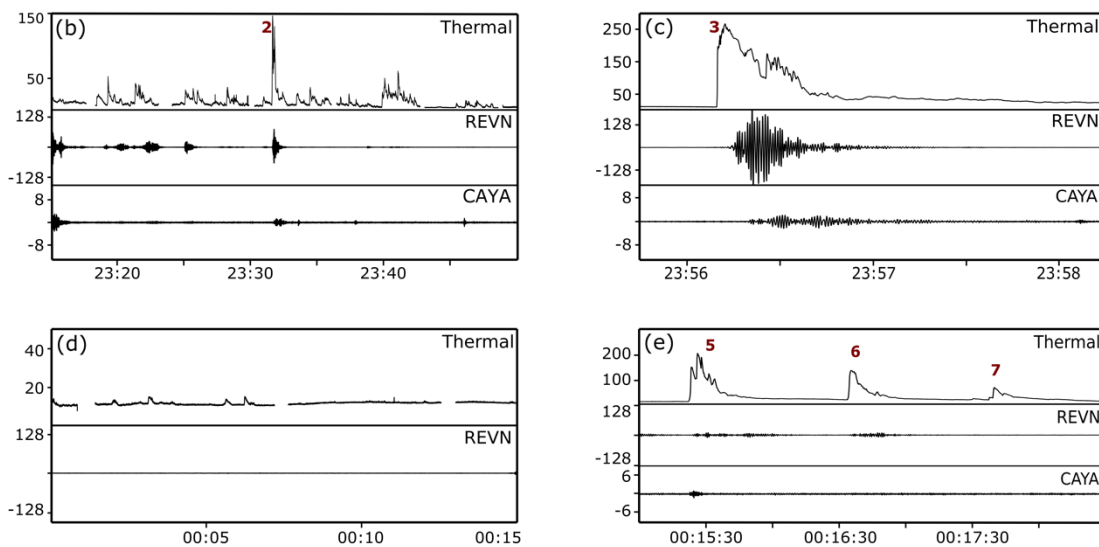
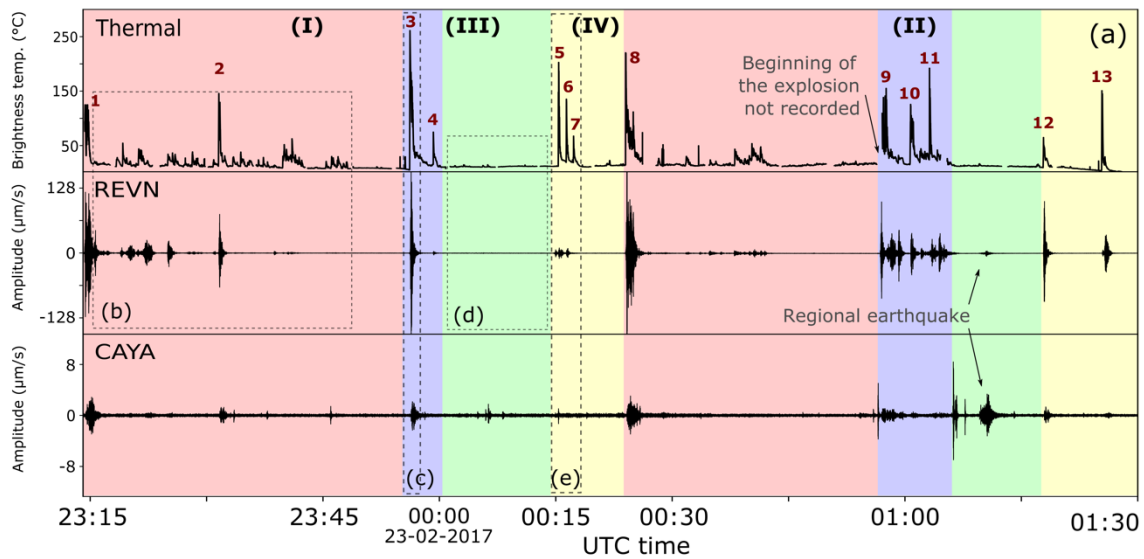
310

311

312

313

Fig. 6 Thermal and seismic waveforms for (a) Type A eruptions of Phase 4, (b) Type B eruptions of Phase 2, and (c) Type C eruptions of Phase 1. Thermal images in the right-hand panels correspond to the times shown as numbers (1-13). The thermal waveforms and duration of the Type A explosions in Phase 2 are similar to those of Sakurajima volcano (as plotted in red in a; data from A. Harris: Sakurajima eruption of 2013-07-27). The corresponding thermal images at Sakurajima, taken at similar time intervals as the Reventador (“Rv”) are marked “Sk”. In the case of Type A eruptions during Phase 4 (a), the thermal waveform and duration is comparable with those recorded at Stromboli volcano (“St”) (as plotted in red in a; data from A. Harris: eruption at Stromboli recorded on 2008-06-03). The full videos with corresponding seismic and thermal waveforms from El Reventador can be found in the ESM.

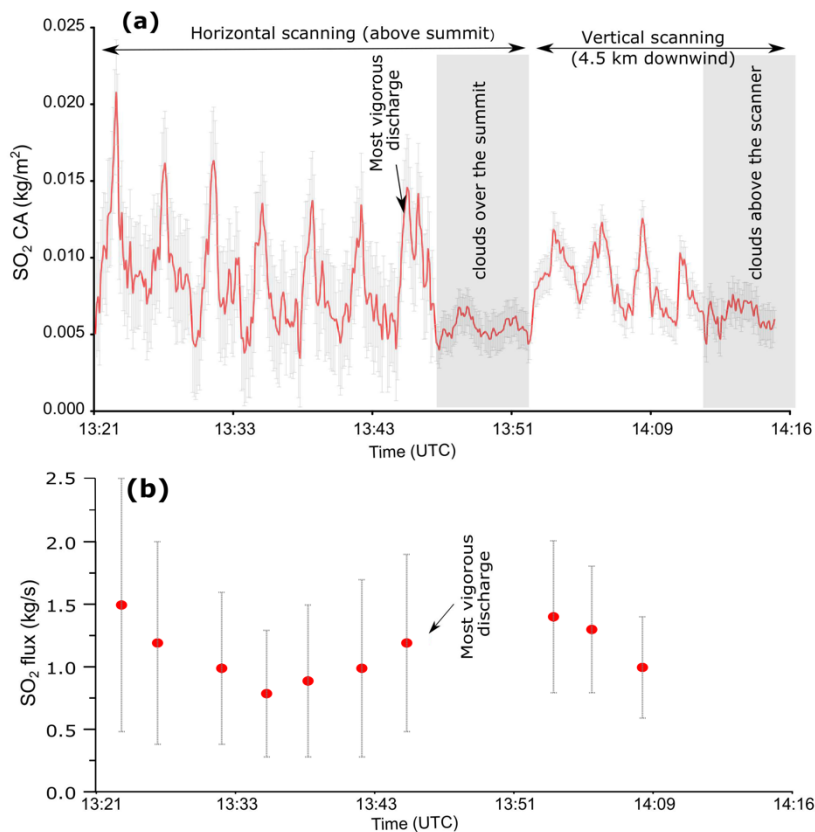


314
 315 **Fig. 7** (a) Temperature time series from region of interest R1 (Fig. 2) and the corresponding seismic
 316 signals from REVN and CAYA (Fig. 1). The main explosions are numbered from 1 to 13. Four distinct
 317 behavior, outlined with different background colors, can be distinguished from the thermal recording,
 318 including (b) a nearly continuous occurrence of Type B and C events, (c) Type A and B events (explosions
 319 3, 9, 10, 11), (d) the low amplitude passive degassing phase; and (e) successive Type A and B event
 320 (explosions 5, 6, 7, 12, 13). Phases I, II, III, and IV occurred successively and repeated themselves once
 321 over the two hours recording, each sequence of phases lasting around one hour and 15 minutes.

322 **SO₂ flux**

323 Figure 8a shows the fluctuation of SO₂ column amount retrieved from the DOAS data. Sunrise
 324 was at about 06h30 (local time), even though light conditions at 08h00 were not optimal for
 325 DOAS measurements, there was sufficient light intensity to perform scanning considering that

326 our system has the capacity to modify automatically the integration time to allow acquisition
 327 of spectra with light intensity within an acceptable range. During our measurements, clouds
 328 started to develop progressively, first around and over the summit then directly above the
 329 scanner, as well as inside the caldera and between our observation site and the vent, forcing
 330 us at first to change the scanning orientation from horizontal to vertical, and finally to end the
 331 measurements. This also caused some periods of unreliable data (Fig. 8a). A mean plume
 332 velocity of 5.6 m s^{-1} was obtained using the thermal infrared camera video, allowing us to
 333 convert to SO_2 flux for approximately one hour of data as reported in Table 1. Fluxes fluctuated
 334 between 0.8 and 1.5 kg s^{-1} with a mean SO_2 emission rate of $1.1 \pm 0.7 \text{ kg s}^{-1}$ (Fig. 8b). The daily
 335 SO_2 emission rate from El Reventador was about 95 ± 60 tons per day during our observation.
 336



337
 338 **Fig. 8** (a) SO_2 column amount (CA) as derived from continuous scanning. The occurrence of clouds that
 339 triggered the shift from horizontal scanning to vertical scanning geometry, as well as the termination
 340 of scanning, is highlighted in gray. (b) The SO_2 flux calculated for each scan shows a cyclic trend despite
 341 the wide margin of errors.

342 Table 1. Results of SO₂ measurements performed on 23 February 2017 using scanning DOAS.

| Scan | Start time (UTC) | End time (UTC) | Projected distance (m) | Number of spectra in the plume | Average column amount (g/m ²) | SO ₂ flux (kg/s) |
|--|------------------|----------------|------------------------|--------------------------------|---|-----------------------------|
| S1 | 13:21 | 13:24 | 1790 | 23 | 0.15 | 1.5 ± 1.0 |
| S2 | 13:24 | 13:27 | 1400 | 18 | 0.14 | 1.2 ± 0.8 |
| S3 | 13:31 | 13:33 | 1326 | 17 | 0.13 | 1.0 ± 0.6 |
| S4 | 13:34 | 13:36 | 1170 | 15 | 0.12 | 0.8 ± 0.5 |
| S5 | 13:38 | 13:41 | 1320 | 17 | 0.12 | 0.9 ± 0.6 |
| S6 | 13:41 | 13:44 | 1560 | 20 | 0.11 | 1.0 ± 0.7 |
| S7 | 13:44 | 13:47 | 1400 | 18 | 0.15 | 1.2 ± 0.7 |
| S8 | 13:47 | 13:50 | | | | |
| S9 | 13:50 | 13:52 | | | | Clouds over the summit |
| S10 | 14:02 | 14:04 | 552 | 24 | 0.35 | 1.4 ± 0.6 |
| S11 | 14:05 | 14:07 | 276 | 12 | 0.35 | 1.3 ± 0.5 |
| S12 | 14:07 | 14:10 | 460 | 20 | 0.32 | 1.0 ± 0.4 |
| S13 | 14:10 | 14:12 | | | | |
| S14 | 14:12 | 14:15 | | | | Clouds above the scanner |
| Mean SO₂ flux estimation: 1.1 ± 0.7 kg/s | | | | | | |

343

344

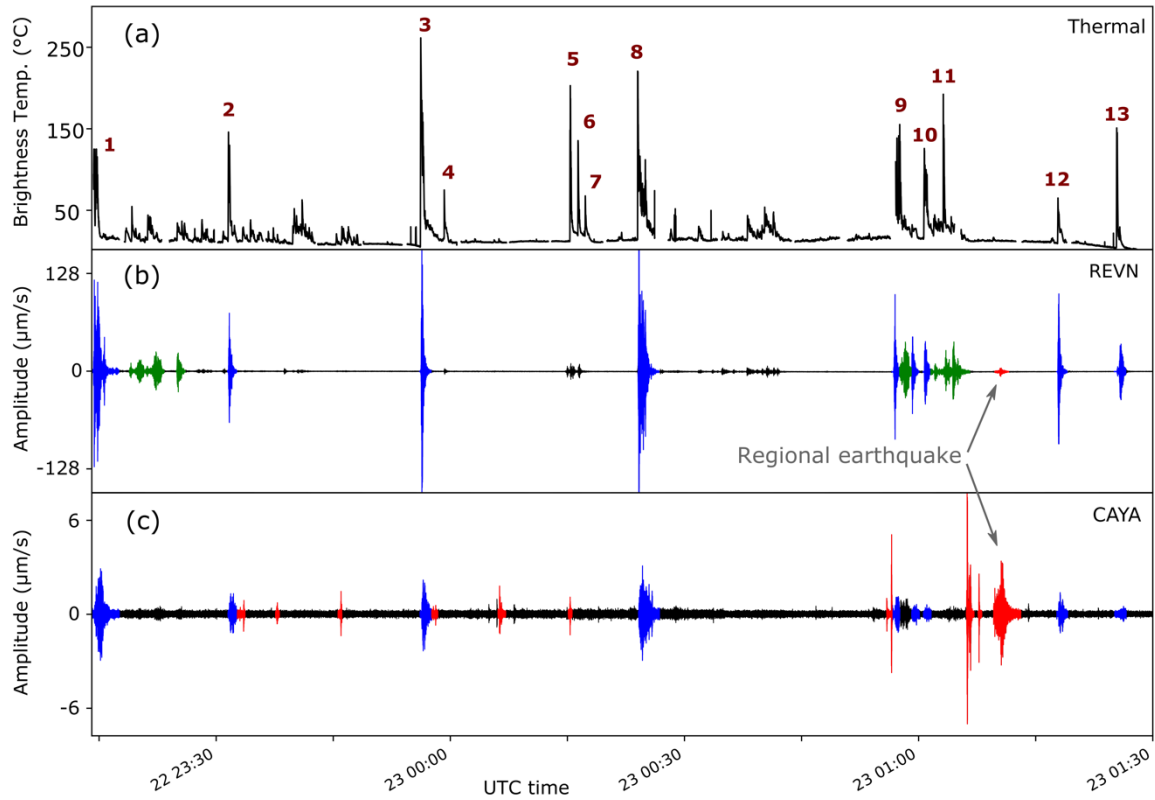
345 Seismicity

346 Using recordings from station REVN (Fig. 1), we identified nine signals that can be considered
 347 as explosion quakes, these are colored in blue in Figure 9. These explosion quakes are also
 348 clearly identified in the recordings of the station CAYA. Ten transient signals observed at CAYA
 349 are unrelated to the activity at El Reventador and are colored in red in Figure 9. These seismic
 350 signals correspond to volcano-tectonic events or ice quakes originating from Cayambe itself.
 351 In addition, three episodes of harmonic tremor were identified at REVN, colored green in
 352 Figure 9. Finally, both stations recorded a regional earthquake whose hypocenter was located
 353 in northern Peru by IGEPN (Fig. 7, Fig. 9).

354

355 The harmonic tremor episodes lasted a few minutes and always appeared after an explosion
 356 quake. All Type A events (explosions 5, 6, 7, 12 and 13) were recorded as low frequency

357 waveforms by the proximal seismic station (REVN) but not all of them appear in the distal
358 (CAYA) seismic recordings (Fig. 9). Thermally, these explosions are associated with the highest
359 energy events and have variable thermal amplitudes. However, these amplitudes are not
360 directly correlated to the amplitude of corresponding seismic signals.

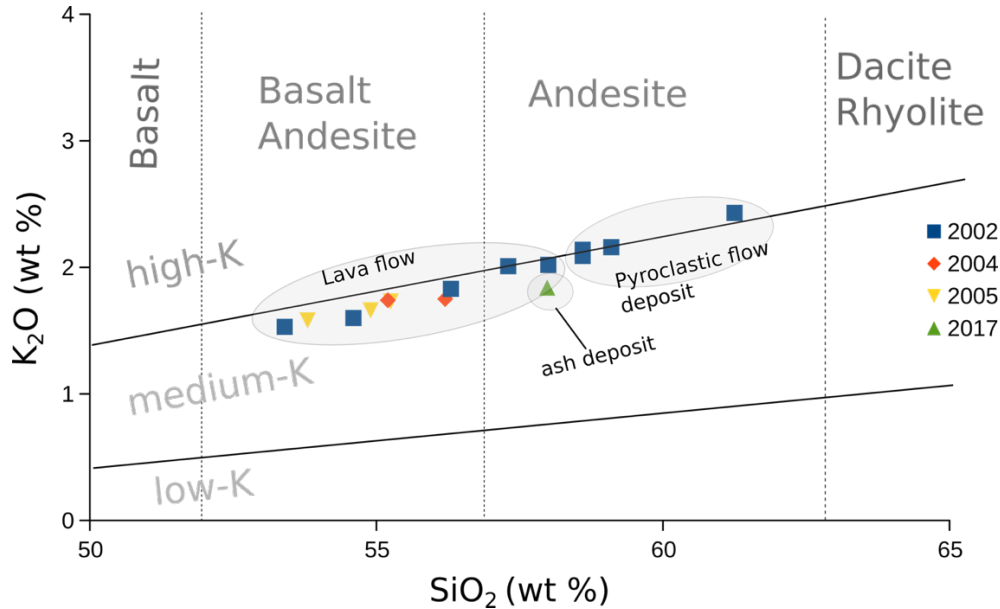


361
362 **Fig. 9** (a) Timeseries of brightness temperature from thermal infrared imagery on which the thirteen
363 Type A and B explosions are identified. (b) Seismic signals from station REVN, located 4 km to the east
364 of the active crater. (c) Seismic signals from station CAYA, located 45 km to the northwest of El
365 Reventador. Most of the explosions that can be identified at the proximal seismic station appear at the
366 distal station as well (marked in blue). The seismic events colored in red are not related to El
367 Reventador activity; they are volcano-tectonic events or ice quakes from Cayambe and a regional
368 earthquake. Harmonic tremor episodes are highlighted in green; and are all preceded by an explosion.
369 The sequence of explosions 5, 6 and 7 produced high thermal amplitudes but low seismicity. Instead,
370 explosions 12 and 13 produced low thermal amplitudes but moderate seismic amplitudes.

371

372 **Bulk Ash composition**

373 The ash is of andesitic composition with SiO₂ contents around 58 wt. % (Table 2). The bulk ash
 374 composition falls in the trend displayed by whole rocks of El Reventador as reported by
 375 Samaniego et al. (2008) (Fig. 10).



376
 377 **Fig. 10** K₂O versus SiO₂ classification diagram (Peccerillo and Taylor 1976) showing the composition of
 378 lavas extruded from El Reventador volcano between 2002 and 2005 (Samaniego et al. 2008) and the
 379 ash sample collected during our observation period.

380 Table 2. Bulk composition of ash samples collected following a Vulcanian explosion at El Reventador
 381 on 22 February 2017.

| SiO ₂ (wt%) | Al ₂ O ₃ (wt%) | Fe ₂ O ₃ (wt%) | MgO (wt%) | CaO (wt%) | Na ₂ O (wt%) | K ₂ O (wt%) | TiO ₂ (wt%) | MnO (wt%) | P ₂ O ₅ (wt%) | Ba (wt%) | Sr (wt%) | Total | H ₂ O (wt%) |
|---------------------------|---|---|--------------|--------------|----------------------------|---------------------------|---------------------------|--------------|--|-------------|-------------|--------|---------------------------|
| 57.98 | 17.67 | 6.93 | 3.76 | 6.73 | 3.57 | 1.84 | 0.88 | 0.11 | 0.37 | 0.14 | 0.10 | 100.08 | 0.24 |

382
 383 **Discussion**

384 Based on coupled patterns in the thermal and seismic waveforms, as well as trends in the SO₂
 385 flux time series, we can group our data into four successive phases (Fig. 7a). We emphasize
 386 that the dynamics presented in this work is representative of our period of observation and
 387 must then be extrapolated with caution, but we believe it gives a useful guide to the dynamics
 388 driving El Reventador’s open-vent persistent explosive activity.

389

390 Phase 1 consists of about 30 minutes of quasi-continuous, minor bursts of gas and ash as seen
391 in the thermal time series as a series of Type C and B events (Fig. 7a; ESM Video 03). These
392 events appear with variable amplitudes in the proximal seismic station but are barely recorded
393 by the distal seismic station (Fig. 7b).

394

395 Phase 2 consists of a single or series of Type A and B explosion(s) that last around two minutes
396 (Fig. 7d; ESM Video 07). These events are clearly distinct from explosions seen in phase 1 as
397 they expel an appreciable quantity of ballistics covering the upper part of the edifice and
398 occasionally generate minor rock falls and pyroclastic density currents (cf. ESM Video 07 and
399 ESM Video 03). Seismicity with high amplitude mirrors the high thermal amplitude signal (Fig.
400 7d). The duration, the waveform and thermal amplitude of the explosions occurring in this
401 phase (Fig. 6a) are similar to those of ash venting occurring at Santiaguito volcano (Johnson et
402 al. 2004; Sahetapy-Engel et al. 2008; Marchetti et al. 2009) and Vulcanian explosions at
403 Sakurajima volcano (Yokoo 2009). Figure 6b shows the comparison between a Type A
404 explosion of Phase 2 at El Reventador and one of Sakurajima's Vulcanian explosion recorded
405 in July 2013 (A. Harris, unpublished data), where the duration and shape of the waveform are
406 similar. We thus interpret these event types to be similar in terms of source, emission and
407 ascent dynamics. We thereby label them "Vulcanian" and assume they are related to stick-slip
408 of a highly viscous plug as at Santiaguito (cf. Bluth and Rose 2004; Sahetapy-Engel et al. 2008)
409 or, more likely, failure of a high viscosity cap in the true Vulcanian sense (Johnson and Lees
410 2000; Hall et al. 2015)

411

412 Phase 3 consists of 10 to 15 minutes of passive degassing (Fig. 7c; ESM Videos 08 and 09).
413 During this phase no explosions are recorded, either in the thermal or seismic records (n.b.,
414 signals registered at the CAYA station are not associated with El Reventador).

415

416 Finally, phase 4 consists of a period of about 10 minutes in which we record a series of Type B
417 explosions (Fig. 7d; ESM Videos 10, 18 and 19). The seismic amplitude of these events is very
418 small when compared to the seismic amplitude associated with the explosions recorded in
419 phases 1 and 2 (Fig. 6) and is the only case where seismic and thermal signals are decoupled.
420 The waveform of the thermal signal and the duration of the individual explosions in this phase
421 (Fig. 6) are comparable to those observed in explosions at Stromboli (e.g. Harris and Ripepe

422 2007a; Harris et al. 2012; Patrick et al. 2005) and Villarrica (Marchetti et al. 2009), as shown
423 in Figure 6c. We thus interpret these event types to be similar in terms of source, emission
424 and ascent dynamics. We thereby label them “Strombolian” and assume they are related to
425 bubble bursting at a relatively low viscosity surface (Shinohara 2005; Patrick et al. 2007) or at-
426 least one that is thinly capped (Gurioli et al. 2014).

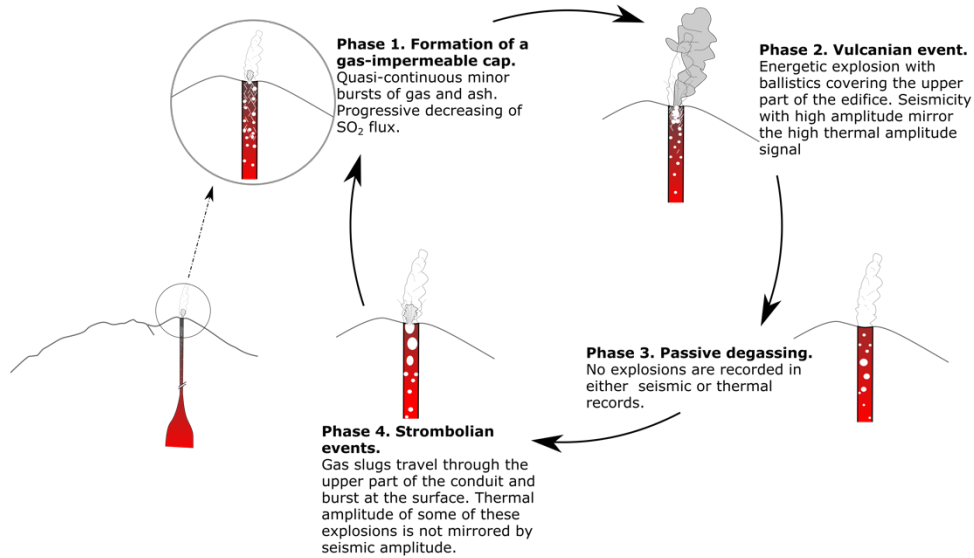
427

428 Activity developed through these four phases twice during the two-hour observation period.
429 Although the SO₂ flux measurements could not be obtained concurrently (DOAS
430 measurements rely on good sunlight while thermal measurements are best performed at
431 night), they also oscillate over a timescale of about one hour thus following the same timescale
432 of trend observed in the thermal and seismic recordings by visual observations.

433

434 Phase 1 characteristics can be interpreted as a conduit which is mostly plugged, or in the
435 process of plug development. Degassing occurs as short bursts of “ash venting” associated
436 with thermal and seismic signals and decreases over time, potentially indicating progressive
437 sealing of the system. Ash venting may be the result of stick-slip events impacting the
438 developing plug (cf. Neuberg 2000; Lensky et al. 2008). Such process can lead to a decrease in
439 the permeability of the upper part of the conduit and, subsequently, to an increase in the
440 pressurization of the system. The progressive decrease of the SO₂ flux, as evidenced in this
441 work, further supports this observation. Phase 1 would hence correspond to the formation of
442 a gas-impermeable cap in the upper part of the conduit (Del Bello et al. 2015; Capponi et al.
443 2016), probably caused by cooling and degassing of the shallowest portion of the magma
444 column, which induces a rheological stiffening and increases magma viscosity (Gurioli et al.
445 2014). The energetic Type A explosion(s) characterizing phase 2 (Fig. 6a), can be interpreted
446 as the culmination of pressure accumulation in the conduit, an accumulation which is finally
447 released by one or a series of energetic explosions (Fig. 7a) destroying the cap. This model is
448 consistent with the ejection of ballistics, the high amplitudes in both the thermal and seismic
449 signals and the similarity with waveforms recorded during “Vulcanian” events at other
450 systems (cf. Fig. 6). During phase 3, which is explosion-free, unhindered degassing occurs, and
451 is interpreted as a period of purely open vent (uncapped) activity. Finally, in phase 4, with the
452 system still in an open-vent configuration, gas slugs can travel through the upper part of the
453 conduit and burst at the free surface producing intermittent “Strombolian” explosions. The

454 thermal amplitude of some of these explosions is not mirrored by the seismic amplitude,
455 possibly because of a source at a shallower level than those with appreciable seismic
456 amplitude at both proximal and distal stations (Fig. 7e). Our thermal, seismic and, to a lesser
457 extent, SO₂ flux observations therefore highlight cyclic transitions at El Reventador between
458 plugged and open vent configurations (Fig. 11).



459
460 **Fig. 11** In this work, the dynamics of El Reventador's activity can be characterised by 4 distinct phases:
461 the formation of a gas-impermeable cap, the phase of Vulcanian explosions, a period of passive
462 degassing and a phase of Strombolian explosions. This last phase gradually fades away as the
463 permeability in the vent decreases and the impermeable cap starts to form.

464

465 **Conclusion**

466 Our analysis of thermal, seismic, and SO₂ flux measurements at El Reventador clearly
467 highlights the temporal succession of different types of explosive and degassing activity that
468 can be classified into four phases. Phase 1 is characterized by frequent, nearly continuous,
469 explosions of small thermal and seismic amplitude diminishing with time, indicating the
470 progressive self-sealing of the conduit. This restricts the gas flow and builds up pressure in the
471 conduit. Phase 2 is characterized by one or several large explosions, associated with high
472 thermal and seismic amplitudes and durations, indicating the destruction of the impermeable
473 cap created during phase 1. Phase 3 is characterized by passive, unhindered degassing
474 indicating entirely open vent conditions while phase 4 sees the episodic bursting of
475 presumably isolated gas slugs at the surface. The entire sequence is repeated twice in a two-

476 hour observation period suggesting a cyclic oscillation between plugged and open vent
477 configurations at El Reventador. The similarity with thermal and seismic waveforms from
478 other classic Strombolian and Vulcanian (VEI 2 through 4) systems suggests the operation of
479 common and globally applicable degassing and explosive processes that cause caps to develop
480 and decay, thereby driving changes in eruption style.

481

482 **Acknowledgements**

483 Fieldwork for this research was conducted as part of the “Trail By Fire” expedition (PI: Y.M.)
484 supported by the Royal Geographical Society (with the Institute of British Geographers)
485 through the Land Rover Bursary; the Deep Carbon Observatory DECADE Initiative; Ocean
486 Optics; Crowcon; Air Liquide; Thermo Fisher Scientific; Cactus Outdoor; Turbo Ace and Team
487 Black Sheep. F.V. acknowledges support from the Region Auvergne Rhone Alpes through its
488 call for projects Pack Ambition Recherche 2018 (project OROVOLC, PI: Y.M.). We thank IGEPN
489 for kindly providing seismic data for this study. This research has been conducted in the
490 context of the Laboratoire Mixte International “Séismes et Volcans dans les Andes du Nord”
491 of IRD. We also thank Sylvie Vergnolle, the Associate Editor, and the anonymous reviewers
492 for their constructive comments that improved this paper.

493

494 **Bibliography**

495 Almeida M, Gaunt H, Ramón P (2019) Ecuador’s El Reventador Volcano Continually Remakes
496 Itself. *Eos* 100:. <https://doi.org/10.1029/2019EO117105>
497 Arellano SR, Hall M, Samaniego P, et al (2008) Degassing patterns of Tungurahua volcano
498 (Ecuador) during the 1999–2006 eruptive period, inferred from remote spectroscopic
499 measurements of SO₂ emissions. *J Volcanol Geotherm Res* 176:151–162.
500 <https://doi.org/10.1016/j.jvolgeores.2008.07.007>
501 Arnold DWD, Biggs J, Anderson K, et al (2017) Decaying Lava Extrusion Rate at El
502 Reventador Volcano, Ecuador, Measured Using High-Resolution Satellite Radar: DECAYING
503 LAVA EXTRUSION AT EL REVENTADOR. *J Geophys Res Solid Earth* 122:9966–9988.
504 <https://doi.org/10.1002/2017JB014580>
505 Bani P (2012) First estimate of volcanic SO₂ budget for Vanuatu island arc. *J Volcanol*
506 *Geotherm Res* 11
507 Bani P, Harris AJL, Shinohara H, Donnadieu F (2013a) Magma dynamics feeding Yasur’s

508 explosive activity observed using thermal infrared remote sensing: YASUR THERMAL
509 SENSING. *Geophys Res Lett* 40:3830–3835. <https://doi.org/10.1002/grl.50722>

510 Bani P, Surono, Hendrasto M, et al (2013b) Sulfur dioxide emissions from Papandayan and
511 Bromo, two Indonesian volcanoes. *Nat Hazards Earth Syst Sci* 13:2399–2407.
512 <https://doi.org/10.5194/nhess-13-2399-2013>

513 Battaglia J, Hidalgo S, Bernard B, et al (2019) Autopsy of an eruptive phase of Tungurahua
514 volcano (Ecuador) through coupling of seismo-acoustic and SO₂ recordings with ash
515 characteristics. *Earth Planet Sci Lett* 511:223–232. <https://doi.org/10.1016/j.epsl.2019.01.042>

516 Bluth GJS, Rose WI (2004) Observations of eruptive activity at Santiaguito volcano,
517 Guatemala. *J Volcanol Geotherm Res* 136:297–302.
518 <https://doi.org/10.1016/j.jvolgeores.2004.06.001>

519 Bogumil K, Orphal J, Homann T, et al (2003) Measurements of molecular absorption spectra
520 with the SCIAMACHY pre-flight model: instrument characterization and reference data for
521 atmospheric remote-sensing in the 230–2380 nm region. *J Photochem Photobiol Chem*
522 157:167–184. [https://doi.org/10.1016/S1010-6030\(03\)00062-5](https://doi.org/10.1016/S1010-6030(03)00062-5)

523 Capponi A, James MR, Lane SJ (2016) Gas slug ascent in a stratified magma: Implications of
524 flow organisation and instability for Strombolian eruption dynamics. *Earth Planet Sci Lett*
525 435:159–170. <https://doi.org/10.1016/j.epsl.2015.12.028>

526 Clarke AB, Esposti Ongaro T, Belousov A (2015) Vulcanian Eruptions. In: *The Encyclopedia*
527 *of Volcanoes*. Elsevier, pp 505–518

528 Del Bello E, Lane SJ, James MR, et al (2015) Viscous plugging can enhance and modulate
529 explosivity of strombolian eruptions. *Earth Planet Sci Lett* 423:210–218.
530 <https://doi.org/10.1016/j.epsl.2015.04.034>

531 Fagents SA, Wilson L (1993) Explosive volcanic eruptions-VII. The ranges of pyroclasts
532 ejected in transient volcanic explosions. *Geophys J Int* 113:359–370.
533 <https://doi.org/10.1111/j.1365-246X.1993.tb00892.x>

534 Formenti Y, Druitt TH, Kelfoun K (2003) Characterisation of the 1997 Vulcanian explosions
535 of Soufrière Hills Volcano, Montserrat, by video analysis. *Bull Volcanol* 65:587–605.
536 <https://doi.org/10.1007/s00445-003-0288-8>

537 Gaunt HE, Burgisser A, Mothes PA, et al (2020) Triggering of the powerful 14 July 2013
538 Vulcanian explosion at Tungurahua Volcano, Ecuador. *J Volcanol Geotherm Res* 392:106762.
539 <https://doi.org/10.1016/j.jvolgeores.2019.106762>

540 Gonnermann HM, Manga M (2003) Explosive volcanism may not be an inevitable consequence
541 of magma fragmentation. *Nature* 426:432–435. <https://doi.org/10.1038/nature02138>

542 Gurioli L, Colo' L, Bollasina AJ, et al (2014) Dynamics of Strombolian explosions: Inferences
543 from field and laboratory studies of erupted bombs from Stromboli volcano: DYNAMICS OF
544 STROMBOLIAN EXPLOSIONS. *J Geophys Res Solid Earth* 119:319–345.
545 <https://doi.org/10.1002/2013JB010355>

546 Hall M, Ramón P, Mothes P, et al (2004) Volcanic eruptions with little warning: the case of
547 Volcán Reventador's Surprise November 3, 2002 Eruption, Ecuador. *Rev Geológica Chile*
548 31:349–358. <https://doi.org/10.4067/S0716-02082004000200010>

549 Hall ML, Steele AL, Bernard B, et al (2015) Sequential plug formation, disintegration by
550 Vulcanian explosions, and the generation of granular Pyroclastic Density Currents at
551 Tungurahua volcano (2013–2014), Ecuador. *J Volcanol Geotherm Res* 306:90–103.
552 <https://doi.org/10.1016/j.jvolgeores.2015.09.009>

553 Harris A (2013) *Thermal Remote Sensing of Active Volcanoes: A User's Manual*. Cambridge
554 University Press

555 Harris A, Ripepe M (2007a) Synergy of multiple geophysical approaches to unravel explosive
556 eruption conduit and source dynamics – A case study from Stromboli. *Geochemistry* 67:1–35.
557 <https://doi.org/10.1016/j.chemer.2007.01.003>

558 Harris A, Ripepe M (2007b) Temperature and dynamics of degassing at Stromboli. *J Geophys*
559 *Res* 112:B03205. <https://doi.org/10.1029/2006JB004393>

560 Harris AJL, Ripepe M, Calvari S, et al (2008) The 5 April 2003 Explosion of Stromboli: Timing
561 of Eruption Dynamics Using Thermal Data. In: *The Stromboli Volcano: An Integrated Study*
562 *of the 2002–2003 Eruption*. American Geophysical Union (AGU), pp 305–316

563 Harris AJL, Ripepe M, Hughes EA (2012) Detailed analysis of particle launch velocities, size
564 distributions and gas densities during normal explosions at Stromboli. *J Volcanol Geotherm*
565 *Res* 231–232:109–131. <https://doi.org/10.1016/j.jvolgeores.2012.02.012>

566 Harris AJL, Thornber CR (1999) Complex effusive events at Kīlauea as documented by the
567 GOES satellite and remote video cameras. *Bull Volcanol* 61:14

568 Hidalgo S, Battaglia J, Arellano S, et al (2015) SO₂ degassing at Tungurahua volcano (Ecuador)
569 between 2007 and 2013: Transition from continuous to episodic activity. *J Volcanol Geotherm*
570 *Res* 298:1–14. <https://doi.org/10.1016/j.jvolgeores.2015.03.022>

571 Instituto Geofísico EPN (2010) Informe de la actividad del volcán El Reventador durante el año
572 2009. Instituto Geofísico de la Escuela Politécnica Nacional

573 Instituto Geofísico EPN (2018) Informe Especial N°2 del volcán El Reventador – 2018.
574 Instituto Geofísico de la Escuela Politécnica Nacional

575 Instituto Geofísico EPN (2019) Informe anual del volcán El Reventador – 2018. Instituto

576 Geofísico de la Escuela Politécnica Nacional

577 Johnson JB, Harris AJL, Sahetapy-Engel STM, et al (2004) Explosion dynamics of pyroclastic
578 eruptions at Santiaguito Volcano: DYNAMICS OF SANTIAGUITO PYROCLASTIC
579 ERUPTIONS. *Geophys Res Lett* 31:n/a-n/a. <https://doi.org/10.1029/2003GL019079>

580 Johnson JB, Lees JM (2000) Plugs and chugs—seismic and acoustic observations of degassing
581 explosions at Karymsky, Russia and Sangay, Ecuador. *J Volcanol Geotherm Res* 101:67–82.
582 [https://doi.org/10.1016/S0377-0273\(00\)00164-5](https://doi.org/10.1016/S0377-0273(00)00164-5)

583 Johnson JB, Lees JM, Gerst A, et al (2008) Long-period earthquakes and co-eruptive dome
584 inflation seen with particle image velocimetry. *Nature* 456:377–381.
585 <https://doi.org/10.1038/nature07429>

586 Kraus S (2006) DOASIS a framework design for DOAS. PhD Thesis, Technische Informatik,
587 Univ.\ Mannheim

588 Lees JM, Johnson JB, Ruiz M, et al (2008) Reventador Volcano 2005: Eruptive activity inferred
589 from seismo-acoustic observation. *J Volcanol Geotherm Res* 176:179–190.
590 <https://doi.org/10.1016/j.jvolgeores.2007.10.006>

591 Lensky NG, Sparks RSJ, Navon O, Lyakhovsky V (2008) Cyclic activity at Soufrière Hills
592 Volcano, Montserrat: degassing-induced pressurization and stick-slip extrusion. *Geol Soc Lond*
593 *Spec Publ* 307:169–188. <https://doi.org/10.1144/SP307.10>

594 Marchetti E, Ripepe M, Harris AJL, Delle Donne D (2009) Tracing the differences between
595 Vulcanian and Strombolian explosions using infrasonic and thermal radiation energy. *Earth*
596 *Planet Sci Lett* 279:273–281. <https://doi.org/10.1016/j.epsl.2009.01.004>

597 Matsushima N (2005) H₂O emission rate by the volcanic plume during the 2000-2002
598 Miyakejima volcanic activity: 2000-2002 MIYAKEJIMA VOLCANIC ACTIVITY. *Geophys*
599 *Res Lett* 32:n/a-n/a. <https://doi.org/10.1029/2005GL023217>

600 Mercalli G (1907) Vulcani attivi della terra: morfologia–dinamismo–prodotti–distribuzione
601 geografica–cause...

602 Miwa T, Toramaru A (2013) Conduit process in vulcanian eruptions at Sakurajima volcano,
603 Japan: Inference from comparison of volcanic ash with pressure wave and seismic data. *Bull*
604 *Volcanol* 75:685. <https://doi.org/10.1007/s00445-012-0685-y>

605 Morrissey M, Mastig L (1999) Vulcanian eruptions. In: *Encyclopedia of Volcanoes*, 1st edn.
606 San Diego, California, USA, pp 463–475

607 Naranjo MF, Ebmeier SK, Vallejo S, et al (2016) Mapping and measuring lava volumes from
608 2002 to 2009 at El Reventador Volcano, Ecuador, from field measurements and satellite remote
609 sensing. *J Appl Volcanol* 5:8. <https://doi.org/10.1186/s13617-016-0048-z>

610 Neuberg J (2000) Characteristics and causes of shallow seismicity in andesite volcanoes. *Philos*
611 *Trans R Soc Lond Ser Math Phys Eng Sci* 358:1533–1546.
612 <https://doi.org/10.1098/rsta.2000.0602>

613 Newhall CG, Self S (1982) The volcanic explosivity index (VEI) an estimate of explosive
614 magnitude for historical volcanism. *J Geophys Res* 87:1231.
615 <https://doi.org/10.1029/JC087iC02p01231>

616 Ortiz HD, Matoza RS, Garapaty C, et al (2020) Multi-year regional infrasound detection of
617 Tungurahua, El Reventador, and Sangay volcanoes in Ecuador from 2006 to 2013. *Acoustics*
618 *Virtually Everywhere*, p 022003

619 Patrick MR, Hams A, Jonathan Dehn Luke Flynn William Gersch Robert Wright C (2005)
620 *Strombolian Eruption Dynamics From Thermal (FLIR) Video Imagery*

621 Patrick MR, Harris AJL, Ripepe M, et al (2007) Strombolian explosive styles and source
622 conditions: insights from thermal (FLIR) video. *Bull Volcanol* 69:769–784.
623 <https://doi.org/10.1007/s00445-006-0107-0>

624 Peccerillo A, Taylor SR (1976) Geochemistry of eocene calc-alkaline volcanic rocks from the
625 Kastamonu area, Northern Turkey. *Contrib Mineral Petrol* 58:63–81.
626 <https://doi.org/10.1007/BF00384745>

627 Platt U, Stutz J (2008) *Differential optical absorption spectroscopy: principles and applications ;*
628 *with 55 tables.* Springer, Berlin

629 Ramon P, Vallejo S, Mothes P, et al (2021) Instituto Geofísico – Escuela Politécnica Nacional,
630 the Ecuadorian Seismology and Volcanology Service. *Volcanica* 4:93–112.
631 <https://doi.org/10.30909/vol.04.S1.93112>

632 Ripepe M, Harris AJL, Marchetti E (2005) Coupled thermal oscillations in explosive activity
633 at different craters of Stromboli volcano: COUPLED THERMAL OSCILLATIONS AT
634 DIFFERENT CRATERS. *Geophys Res Lett* 32:. <https://doi.org/10.1029/2005GL022711>

635 Sahetapy-Engel ST, Harris AJL (2009) Thermal-image-derived dynamics of vertical ash
636 plumes at Santiaguito volcano, Guatemala. *Bull Volcanol* 71:827–830.
637 <https://doi.org/10.1007/s00445-009-0284-8>

638 Sahetapy-Engel ST, Harris AJL, Marchetti E (2008) Thermal, seismic and infrasound
639 observations of persistent explosive activity and conduit dynamics at Santiaguito lava dome,
640 Guatemala. *J Volcanol Geotherm Res* 173:1–14.
641 <https://doi.org/10.1016/j.jvolgeores.2007.11.026>

642 Samaniego P, Eissen J-P, Le Pennec J-L, et al (2008) Pre-eruptive physical conditions of El
643 Reventador volcano (Ecuador) inferred from the petrology of the 2002 and 2004–05 eruptions.

644 J Volcanol Geotherm Res 176:82–93. <https://doi.org/10.1016/j.jvolgeores.2008.03.004>

645 Self S, Wilson L, Nairn IA (1979) Vulcanian eruption mechanisms. *Nature* 277:440–443.

646 <https://doi.org/10.1038/277440a0>

647 Shinohara H (2005) Volcanic gases emitted during mild Strombolian activity of Villarrica

648 volcano, Chile. *Geophys Res Lett* 32:L20308. <https://doi.org/10.1029/2005GL024131>

649 Siebert L, Simkin T, Kimberly P (2011) *Volcanoes of the World: Third Edition*. University of

650 California Press

651 Sparks RSJ (1997) Causes and consequences of pressurisation in lava dome eruptions. *Earth*

652 *Planet Sci Lett* 150:177–189. [https://doi.org/10.1016/S0012-821X\(97\)00109-X](https://doi.org/10.1016/S0012-821X(97)00109-X)

653 Thivet S, Harris AJL, Gurioli L, et al (2021) Multi-Parametric Field Experiment Links

654 Explosive Activity and Persistent Degassing at Stromboli. *Front Earth Sci* 9:669661.

655 <https://doi.org/10.3389/feart.2021.669661>

656 Voigt S, Orphal J, Bogumil K, Burrows JP (2001) The temperature dependence (203–293 K)

657 of the absorption cross sections of O₃ in the 230–850 nm region measured by Fourier-transform

658 spectroscopy. *J Photochem Photobiol Chem* 143:1–9. [https://doi.org/10.1016/S1010-](https://doi.org/10.1016/S1010-6030(01)00480-4)

659 [6030\(01\)00480-4](https://doi.org/10.1016/S1010-6030(01)00480-4)

660 Wilson L, Self S (1980) Volcanic explosion clouds: Density, temperature, and particle content

661 estimates from cloud motion. *J Geophys Res* 85:2567.

662 <https://doi.org/10.1029/JB085iB05p02567>

663 Woods AW (1995) A model of vulcanian explosions. *Nucl Eng Des* 155:345–357.

664 [https://doi.org/10.1016/0029-5493\(94\)00881-X](https://doi.org/10.1016/0029-5493(94)00881-X)

665 Yokoo A (2009) Continuous thermal monitoring of the 2008 eruptions at Showa crater of

666 Sakurajima volcano, Japan. *Earth Planets Space* 61:1345–1350.

667 <https://doi.org/10.1186/BF03352987>

668